SIMULATING SPACE WEATHERING IN THE TRANSMISSION ELECTRON MICROSCOPE VIA DYNAMIC IN SITU HEATING AND HELIUM IRRADIATION OF OLIVINE. M. S. Thompson[1], P. Haenecour[2], J. Y. Howe[3,4], D. L. Laczniak[1], T. J. Zega[2], J. Hu[5], W. Chen[5], L. P. Keller[6] and R. Christoffersen[7]. [1]Department of Earth, Atmospheric, and Planetary Sciences, Purdue University, West Lafayette, IN, 47907, mthompson@purdue.edu [2]Lunar and Planetary Laboratory, University of Arizona, Tucson, AZ, 85721, [3]Hitachi High Technologies America Inc., Clarksburg, MD, 20871, [4]Department of Materials Science and Engineering, University of Toronto, Toronto, ON, M5S 3E4, [5]Intermediate Voltage Electron Microscopy - Tandem Facility, Argonne National Laboratory, Argonne, IL, 60439, [6]ARES, NASA Johnson Space Center, Houston, TX, 77058, [7]Jacobs, NASA Johnson Space Center, Houston, TX, 77058.

Introduction: The chemical composition, microstructure, and optical properties of grains on the surfaces of airless bodies are predominantly altered by micrometeorite impacts and solar wind irradiation. These processes drive space weathering and result in the formation of features including chemically-altered, amorphous grain rims, Fe nanoparticles (npFe), and vesiculated grain textures [1]. These characteristics have been identified in returned samples from the surfaces of the Moon and asteroid Itokawa, e.g., [2,3].

In order to advance our understanding of the formation of these microstructural and chemical features in returned samples, we have simulated space weathering processes for a variety of materials via laboratory experiments. These experiments include ion irradiation to simulate solar wind exposure and laser irradiation and in situ heating to simulate micrometeorite impacts, e.g., [4,5]. While these experiments have provided considerable insight into the formation mechanisms of many space weathering features, they are predominantly static and typically performed separately. Here we present results from the simulated space weathering of olivine grains via He irradiation and dynamic heating, both performed *in situ* inside the transmission electron microscope (TEM). These experiments allow for the real-time observation of chemical and microstructural changes resulting from the superposed effects of ion irradiation and pulsed heating..

Methods: Grains of San Carlos olivine were drop-cast onto C-coated Cu TEM grids and SiN MEMS-based heating chips (Norcada) for analysis in the TEM. We performed in situ irradiation experiments using 12 keV He ions at the intermediate-voltage electron microscope tandem facility (IVEM) at Argonne National Laboratory. We irradiated three individual samples, each at a flux of $3x10^{12}$ ion/cm^2/s up to total fluences of $3.5x10^{16}$ ions/cm^2, $5x10^{16}$ ions/cm^2, and $8x10^{16}$ ions/cm^2, respectively. After irradiation, we then performed rapid in situ heating of the $8x10^{16}$ ions/cm^2 sample, at a rate of 100ºC per second, up to 1000ºC and immediately returning to room temperature.

We imaged each sample before, throughout, and after the completion of irradiation and/or heating in the 300 kV Hitachi 9000 TEM at Argonne National Lab. After in situ irradiation and heating, we performed secondary electron imaging to investigate the nature of the grain surfaces. We also performed energy-dispersive x-ray spectroscopy (EDS) to obtain chemical maps using the Hitachi SU 9000/transmission scanning electron microscope (STEM) at the University of Arizona.

Results and Discussion: We imaged samples at various stages of the irradiation and heating process.

$3.5x10^{16}$ ions/cm^2 Sample: At this irradiation fluence we begin to observe the formation of vesicles around the outer margins of grains, readily visible in secondary electron (SE) and annular dark field (ADF) scanning TEM (STEM) images (Fig. 1a-b). SE images reveal depressions on the grain surface which correlate to the size and location of vesicles in the ADF images, indicating that they are concentrated in the outermost grain rims. These vesicles range in size from a few nm to ~40 nm in size. We estimate these vesicles are in the upper ~80-100 nm of the olivine surface, based on calculations

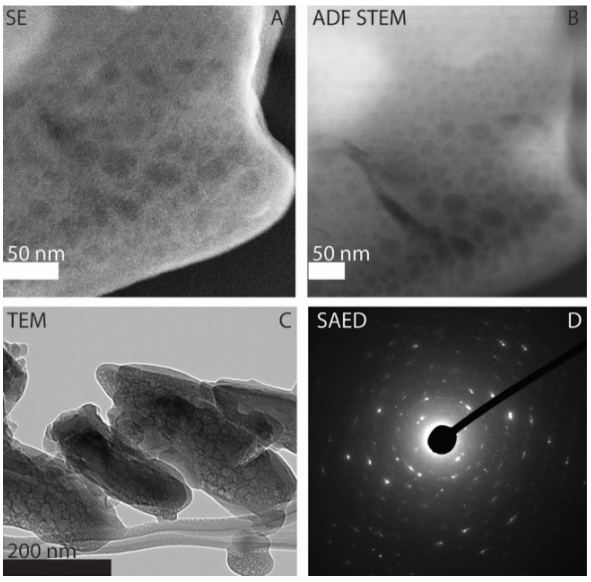

Figure 1: TEM data of grains after irradiation. A) SE image of the 3.5 x 10^{16} ions/cm^2 irradiated grain showing surface depressions corresponding to vesicles in the B) ADF image. C) TEM image of vesicles in the sample irradiated to $5x10^{16}$ ions/cm^2 and D) Selected-area electron diffraction pattern containing discrete reflections and rings, indicating the start of amorphization.

from the Stopping and Range of Ions in Matter (SRIM) code [6]. These features appear similar in size to vesicles observed on the surfaces of grains returned from asteroid Itokawa [3]. The fluences experienced by the grains in this experiment translate to ~10-100 years on an airless surface at 1 AU, within range of the exposure timescales estimated for Itokawa grains from solar flare track analyses [7]. These results suggest solar wind implantation may be a viable mechanism for vesicle development, even over short timescales.

$5x10^{16}$ ions/cm^2 Sample: We observe the widespread distribution of vesicles with larger average size than those observed at lower fluences, up to ~60 nm in size (Fig. 1c). SAED patterns indicate the grains are beginning to amorphize (Fig. 1d). This breakdown of crystal structure begins at the critical amorphization fluence proposed in [8]. The amorphization does not proceed to completion, as the stopping range of the He ions in this experiment is less than the thickness of the grains, and because He likely only causes partial amorphization in regions other than the outermost few nm [6].

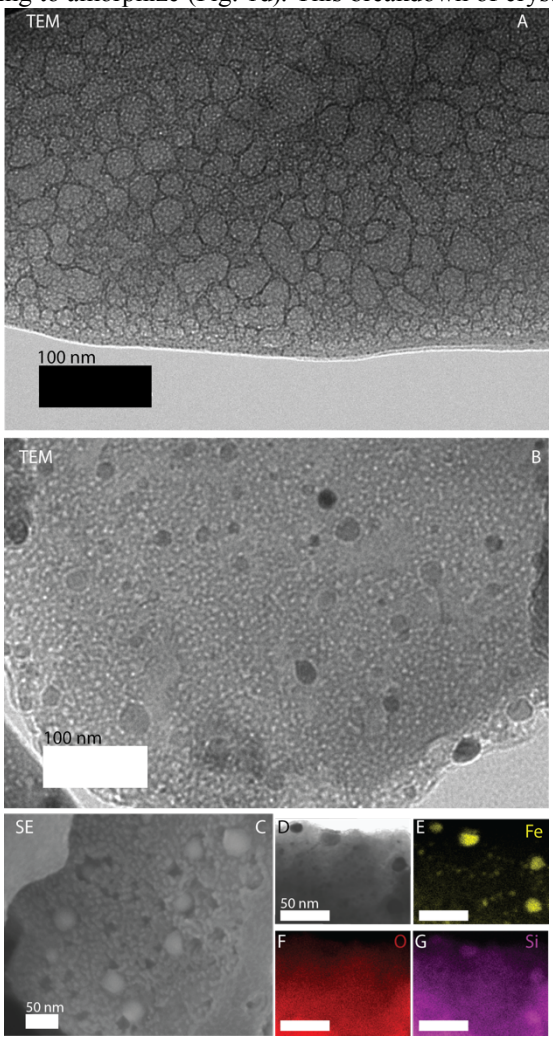

Figure 2: A) TEM image of vesicles after $8x10^{16}$ ions/cm^2 irradiation. B) TEM image of smaller vesicles and the presence of nanoparticles after flash heating. C) SE image of the grain after heating showing nanoparticles and pitted texture on the surface. D) Nanoparticle-bearing rim. E-G) EDS maps for Fe, O, and Si showing the composition of the nanoparticles and the matrix.

$8x10^{16}$ ions/cm^2 Sample: At the highest irradiation fluence we observe vesicles increasing in size, up to ~100 nm in diameter (Fig. 2a). After flash heating, the overall size of the vesicles decreases substantially to <10 nm, and become much more uniform. In addition, we observe the formation of nanoparticles throughout the sample, ranging from a few nm to 30 nm in diameter (Fig. 2b). SE images of the heated sample shows that some of these nanoparticles are on the surface of the grain. The size and distribution of these nanoparticles are similar to in situ heating experiments performed for naturally solar wind irradiated lunar soils [9].

The images also reveal the presence of a pitted texture across localized regions of the grain surface, with the depressions often being associated with surface nanoparticles (Fig. 2c). We hypothesize that these pits result from degassing He as the sample is heated. This loss of He is also likely responsible for the reduction in size of the vesicles. EDS maps of the heated grains show the nanoparticles are enriched in Fe and at least some are also enriched in Si (Fig. 2e-g).

While nanoparticles with Fe-Si composition have been observed in isolated instances in lunar samples [10], Fe^0 nanoparticles (npFe) are the expected formation product of space weathering. However, such nanoparticles are hypothesized to form with solar wind H acting as a reducing agent. The absence of H in our experiment may have prompted the formation of FeSi nanoparticles. Nonetheless, simulating space weathering conditions in situ using dynamic He irradiation and rapid heating produces microstructural and chemical features similar to those observed in returned samples. These results suggest solar wind irradiation is a possible mechanism for the formation of vesicles on the surfaces of grains returned from Itokawa.

References: [1] Pieters C.M. and Noble S.K. (2016) *J. Geophys. Res-Planet., 121,* 1865-1884. [2] Keller L.P. and McKay D.S. (1993) *Science*, *261*, 1305-1307. [3] Noguchi T. et al. (2011) *Science, 333*, 1121-1125. [4] Loeffler, M.J. et al. (2009) *J. Geophys. Res- Planet.*, 114(E3). [5] Sasaki S., et al. (2001) *Nature*, *410*, 555-557. [6] Christoffersen R. and Keller, L.P. (2015) *Space Weathering of Airless Bodies*, Abstract #2992. [7] Keller et al. (2016) *LPS XLVII*, Abstract #2525 [8] Carrez, P. et al. (2002) *Meteorit.Planet. Sci., 37*, 1599-1614. [9] Thompson, M.S. et al. (2017), *Meteorit.Planet. Sci., 52*, 413-427. [10] Anand et al. (2005) *Proc. Nat. Ac. Sci. 101,* 6847–685.